Chemistry of defect induced photoluminescence in chalcopyrites: The case of $CuAlS_2$

Leandro M. Liborio,[1,a] Christine L. Bailey,[2] Giuseppe Mallia,[1] Stanko Tomić,[2] and Nicholas M. Harrison[1,2]
[1]Department of Chemistry, Imperial College London, Thomas Young Centre for the Simulation of Materials, Exhibition Road, London SW7 2AZ, United Kingdom
[2]Department of Computational Science and Engineering, STFC Daresbury Laboratory, Daresbury, Warrington, Cheshire WA4 4AD, United Kingdom

(Received 27 September 2010; accepted 9 December 2010; published online 25 January 2011)

Hybrid exchange density functional theory is used to study the wide band gap chalcopyrite $CuAlS_2$. The formation energies of charged and neutral intrinsic defects are calculated for different environmental conditions, and it is shown that $CuAlS_2$ is a *p*-type material that cannot be type inverted through the formation of intrinsic defects. The calculated band gap states associated with the different intrinsic defects are used to comment on the origin of the observed $CuAlS_2$ photoluminescence emissions. The origin and stability of ordered defect compounds derived from $CuAlS_2$ are investigated, and it is concluded that $CuAl_5S_8$ is a stable ordered defect compound, albeit in a small region of phase space. © *2011 American Institute of Physics*.
[doi:10.1063/1.3544206]

I. INTRODUCTION

The I-III-VI_2 chalcopyrite compounds (I=Cu, Ag; III =Al, Ga, In; and VI=S, Se, Te) have been attracting considerable attention as new materials for optical applications: variations in their composition result in significant changes in their lattice constants and energy gaps. In particular, Cu-III-VI_2 (III=Al, Ga and VI=S, Se) chalcopyrites have energy gaps ranging from 1.70 to 3.49 eV and are, therefore, promising candidates for light-emitting devices operating in the visible and ultraviolet spectral ranges.[1] Among these Cu-III-VI_2 chalcopyrites $CuAlS_2$ has a 3.49 eV room temperature band gap,[2] and its bulk single crystals usually exhibit values of room-temperature *p*-type mobility and hole concentration of the order of 0.9 S cm^{-1} and 5.1×10^{18} cm^{-3}, respectively.[3]

Photoluminescence (PL), high resolution photoreflectance, and time resolved PL experiments reveal the existence of luminescence emissions in $CuAlS_2$ at temperatures ranging from 10 to 300 K.[4,5] It has been suggested that these emissions might be due to: (a) free excitons (FEs), (b) donor and acceptor-bound emissions, and (c) donor-acceptor pair recombination $(\mathbb{D}^+\mathbb{A}^-)$ emissions.[4,5] $(\mathbb{D}^+\mathbb{A}^-)$ and donor-acceptor bound emissions are related to the intermediate optical band gap states that appear in defective $CuAlS_2$ and, therefore, PL emissions related with these excitons have wavelengths smaller than the optical band gap of $CuAlS_2$. In previous works, the orange PL emission observed in $CuAlS_2$ has been linked to a $(\mathbb{D}^+\mathbb{A}^-)$ transition.[4,6] As regards the so-called near-band-edge PL (NBEPL) emission, previous works have attributed it to either FE or defect-bound excitons, whose band gap states are near the valence band maximum (VBM) or the conduction band minimum (CBM).[4,6]

The binding energy of the FE in $CuAlS_2$ is R_x =70 meV,[4] which is larger than the binding energies of other ultraviolet emitting materials such as ZnO (60 meV), ZnS (39 meV), and GaN (21 meV).[7] This binding energy is calculated assuming that: (a) the effective masses of $CuAlS_2$ are given by the average value of the effective masses of $CuGaS_2$, ZnSe, ZnS, $AgGaS_2$, and GaN and (b) the dielectric constant of $CuAlS_2$ is $\varepsilon=7.0\varepsilon_0$.[4] This large binding energy implies that FE in $CuAlS_2$ are stable at 298 K, a feature which means that $CuAlS_2$ has the potential to be a highly efficient ultraviolet emitter at room temperature.

The 3.49 eV optical band gap and the large FE binding energy suggest that $CuAlS_2$ could potentially be used for building blue and green light emitting devices.[8] For producing such devices it is desirable to understand the nature of the PL emissions, which are strongly linked with the defect chemistry of $CuAlS_2$. So far, to the best of the authors knowledge, although there have been a number of experimental studies,[2,6,9–12] there are no theoretical studies on the defect chemistry of $CuAlS_2$. NBEPL emissions have been observed in $CuAlS_2$ powder[6] and epilayers[4] within the 15–298 K temperature range. The intensity of NBEPL related emissions decreases in annealed samples, and the photoemission peaks are shifted toward lower energies. These peaks have been related to the formation of intrinsic defects. When defects are created, emissions related to $(\mathbb{D}^+\mathbb{A}^-)$ pairs and donor-acceptor bound excitons prevail. It has been suggested, for instance, that the 1.9–2.0 eV orange emission is caused by $(\mathbb{D}^+\mathbb{A}^-)$ recombination.[6] In the current work we calculate: (a) the stability of pure $CuAlS_2$ with respect to other competing phases and (b) the stability of different intrinsic defects in $CuAlS_2$. Defects in various possible charge states, such as copper vacancies $(V_{Cu}^{0/1-})$ and sulfur vacancies $(V_S^{0/1+/2+})$, aluminum substituting copper $(Al_{Cu}^{0/1+/2+})$ and copper substituting aluminum $(Cu_{Al}^{0/1-/2-})$ are modeled. More-

[a]Electronic mail: l.liborio@imperial.ac.uk.

 © 2011 American Institute of Physics

Downloaded 02 Feb 2011 to 155.198.39.40. Redistribution subject to AIP license or copyright; see http://jap.aip.org/about/rights_and_permissions

over, the electronic structures associated with these defects and their influence in the PL emissions of $CuAlS_2$ are reported.

Among the $CuAlS_2$ competing phases are the ternary ordered defect compounds (ODCs). These ODCs are complex defect structures that have been observed in several chalcopyrites such as $CuGaSe_2$, $CuGaTe_2$, and $CuInSe_2$,[13,14] and can be thought of as ordered structures of neutral $[2V_{Cu}^{1-}+(Ga/In)_{Cu}^{2+}]^0$ compound defects.[15] The existence of ODCs means that these materials have a structural tolerance to large anion-cation off-stoichiometry, and they do not undergo major structural changes as the composition is varied. The optoelectronic properties also show an unexpectedly weak variation with composition, as the ODCs have similar optoelectronic response to the stoichiometric phases.[14,16,17] In $CuInSe_2$ this is because the $(2V_{Cu}^{1-}+In_{Cu}^{2+})^0$ compound defect is charge compensated, has no deep-gap levels, and thus does not impact in the optoelectronic performance of $CuInSe_2$.[18]

Most of the theoretical works on the ODCs in the literature are limited to ODCs derived from $CuInSe_2$, $CuGaTe_2$, and $CuGaSe_2$;[14,19,18] and the most commonly observed ODCs in these chalcopyrites are $Cu(In/Ga/Al)_5(Se/Te)_8$ and $Cu(In/Ga/Al)_3(Se/Te)_5$. The two ODCs simulated in this work are $CuAl_5S_8$ and $CuAl_3S_5$.

II. METHODOLOGY

A. Computational details

Density functional theory (DFT) calculations were performed using CRYSTAL (Ref. 20) and the B3LYP hybrid exchange functional.[21,22] This functional has been shown to provide a reliable description of the electronic structure, geometry, and energetics in a wide range of materials.[23,24] In particular, hybrid exchange functionals, such as B3LYP, provide a much better prediction of the band gap of semiconductors than local density approximation or generalized gradient approximation DFT functionals.

Polarized triple valence Gaussian basis sets, which have been used in previous studies,[24,25] were used throughout and detailed information is included in Ref. 26. In CRYSTAL, real space summations of the Coulomb and exchange contributions to the Hamiltonian matrix are controlled by five overlap criteria. In these calculations, four of these overlap criteria have values of 10^{-6} and the last one has a value of 10^{-12}. The control of these approximations is described in detail elsewhere.[20] A Monkhorst–Pack shrinking factor of eight was used to sample the first Brillouin zone, and a Gilat net of eight points was used in the evaluation of the Fermi energy and density matrix.[20] Defects were calculated within 64 atom supercells, obtained by doubling the *a* and *b* axes of the conventional cell.

B. Energy correction for charged defects

The use of periodic boundary conditions within electronic structure calculations leads to the conditional convergence of the Coulomb potential. For neutral systems the Ewald summation may be used to ensure that the Coulomb potential and total energies converge to well defined values.[27] In charged systems, however, the total energy can only be calculated to within a constant offset value.[28] This offset is corrected through the electrostatic potential alignment correction (ΔE_v).[28] The ΔE_v correction can be explicitly computed by calculating the change in the energy of the neutral system when an electron is removed from it. When the size of the system tends to infinity, the change in the energy converges to the value of the energy offset. To calculate the value of ΔE_v in $CuAlS_2$, the change in energy between a neutral system, and a system with a single electron removed, was calculated for increasing system size until convergence (to within 0.04 eV) of the energy offset was obtained. The results of these calculations are given in Table I. In this work a 64 atom supercell, obtained by doubling the *a*, *b*, and *c* axes of the primitive lattice, has been adopted. In the calculations of charged defect energies, a value of 6.518 eV is used for ΔE_v for the $CuAlS_2$ system.

TABLE I. Convergence on the value of ΔE_v for increasing system size.

No. of Atoms	ΔE_v (eV)
8	6.220
32	6.520
64	6.518
128	6.523

The *ab initio* calculation of the formation energy of charged defects involves the addition of a uniform background charge to neutralize the cell: The total energy would diverge for a periodically repeating charged system. The total energy of a charged defect in a periodic system includes terms due to defect-defect, defect-background, and background-background Coulomb interactions. The values of these terms are required for the accurate calculation of the energy of an isolated defect and, assuming the defect charge *q* is localized, they can be approximated by the multipole correction,[29]

$$\Delta E = \frac{q^2\alpha_M}{2\varepsilon_r V^{1/3}} + \frac{2\pi qQ}{3\varepsilon_r V} + O(V^{-5/3}), \quad (1)$$

where α_M is the lattice dependent Madelung constant and V is the volume of the supercell. Q is the quadrupole moment of the defect. Finally, ε_r is the static relative dielectric constant, measured in units of the vacuum dielectric constant, ε_0. In this work, an experimental value of $7.0\varepsilon_0$ (Ref. 4) is used for the ε_r in $CuAlS_2$.

Previous theoretical calculations on $CuGaS_2$ used 64 atom unit cells, which were sufficiently large to render the second order term in Eq. (1) as negligible relative to the defect formation energies.[30] In this work a 64 atoms unit cells are used as well and the value of ΔE is also calculated using only the first term in Eq. (1). For a 64 atom supercell, the calculated value of ΔE in $CuAlS_2$ is 0.27 and 1.08 eV for the single and double charged defects.

C. Phase stability

At equilibrium, the Gibbs free energy of $CuAlS_2$ with respect to its elemental solids is given by:

Downloaded 02 Feb 2011 to 155.198.39.40. Redistribution subject to AIP license or copyright; see http://jap.aip.org/about/rights_and_permissions

$$G_{CuAlS_2} = \mu_{Cu} + \mu_{Al} + 2\mu_S. \quad (2)$$

μ_i (i=Cu, Al, S) is the absolute value of the chemical potential of element i. Equation (2) can be rewritten as:

$$\Delta G_{CuAlS_2} = \Delta\mu_{Cu} + \Delta\mu_{Al} + 2\Delta\mu_S, \quad (3)$$

where ΔG_{CuAlS_2} is the Gibbs free energy of formation of $CuAlS_2$ and $\Delta\mu_i(\Delta\mu_i = \mu_i - \mu_i^0)$ is the difference between μ_i and the value of μ_i when the element i is in its standard state. This state is defined at a temperature of 298.15 K and a pressure of 1 atm. The allowed values of μ_i are determined from a set of thermodynamic limits. The upper bound of μ_i is the chemical potential of the corresponding element in its standard state, as to avoid precipitation of the later. That is,

$$\Delta\mu_i \leq 0. \quad (4)$$

We are primarily interested in the region of phase space in which $CuAlS_2$ is stable. In this stability region the chemical potentials of the constituent atoms must equal the Gibbs free energy of formation of the compound, as stated in Eq. (3), and they are further restricted by other competing phases. To identify the stability region of $CuAlS_2$ it is necessary to calculate the relative stability of these competing phases, such as Cu_2S. For instance:

$$2\Delta\mu_{Cu} + \Delta\mu_S \leq \Delta G_{Cu_2S}. \quad (5)$$

The following competing phases have been considered: Cu_2S low chalcocite,[31] Al_2S_3,[32] $CuAl_3S_5$, and $CuAl_5S_8$. The allowed values of $\Delta\mu$ are bound by values that preserve the stability of $CuAlS_2$, avoiding the formation of competing phases.

Gibbs free energies are computationally very expensive to calculate from first principles and, therefore, they are usually approximated.[33–35] In this case, the approximations are applied when defining the variational limits of $\Delta\mu_i$(i =Cu, Al, S), which is done through the formation energies of $CuAlS_2$ and its competing phases. In the following, the methodology is exemplified using the Gibbs formation energy of $CuAlS_2$, which is defined in Eq. (3). This equation can be written as follows:

$$\begin{aligned}\Delta G_{CuAlS_2} &= G_{CuAlS_2} - G_{Al} - G_{Cu} - 2G_S \\ &= E^{DFT}_{CuAlS_2} - E^{DFT}_{Cu} - E^{DFT}_{Al} - 2E^{DFT}_S + F^{vib.}_{CuAlS_2} \\ &\quad - F^{vib.}_{Cu} - F^{vib.}_{Al} - 2F^{vib.}_S + p(V_{CuAlS_2} - V_{Cu} - V_{Al} \\ &\quad - 2V_S). \end{aligned} \quad (6)$$

In this equation, the Gibbs free energy, G=E−TS+pV, is written as

$$G = E^{DFT} + F^{vib.} + pV. \quad (7)$$

E^{DFT} is the *ab initio* total energy of the material, $F^{vib.} = E^{vib.} - TS^{vib.}$ is the *Helmholtz* vibrational energy,[33] which depends on the phonons and is a function of temperature, and pV is the pressure-volume term.

The pV and $F^{vib.}$ terms are small for crystalline incompressible materials such as $CuAlS_2$,[33,35,36] and Eq. (6) uses *differences* between these quantities to define the $\Delta\mu_i$ variational limits. Consequently, the pV and $F^{vib.}$ contributions can be considered as negligible, and ΔG_{CuAlS_2} can be written as:

$$\Delta G_{CuAlS_2} = E^{DFT}_{CuAlS_2} - E^{DFT}_{Cu} - E^{DFT}_{Al} - 2E^{DFT}_S, \quad (8)$$

where $E^{DFT}_{CuAlS_2}$, E^{DFT}_{Cu}, E^{DFT}_{Al}, and E^{DFT}_S are the *ab initio* total energies of these materials in their solid standard states. $E^{DFT}_{CuAlS_2}$ is the total energy of bulk $CuAlS_2$ in its tetragonal phase and E^{DFT}_S is calculated in its pure orthorombic α phase.[37] As regards Cu and Al, the B3LYP approximation does not provide accurate energies for metals and, therefore, E^{DFT}_{Cu} and E^{DFT}_{Al} are calculated using the experimental standard formation enthalpies, ΔH^0, of Al_2S_3 and Cu_2S as,

$$E^{DFT}_{Al} = \frac{1}{2}[E^{DFT}_{Al_2S_3} - 3E^{DFT}_S - \Delta H^0_{Al_2S_3}], \quad (9)$$

$$E^{DFT}_{Cu} = \frac{1}{2}[E^{DFT}_{Cu_2S} - E^{DFT}_S - \Delta H^0_{Cu_2S}]. \quad (10)$$

D. Defect energetics

The formation of a defect can be considered in terms of an exchange between the host material and notional atomic and electronic reservoirs. The formation energy of a defect in the charge state q can be written as

$$\Delta G_{D,q}(E_F,\mu) = G_{D,q} - G_{CuAlS_2} + \Sigma_i n_i \mu_i + q(\Delta E_v + E_F), \quad (11)$$

where $G_{D,q}$ and G_{CuAlS_2} are the Gibbs free energies of $CuAlS_2$ with and without defect D, and they are calculated as described in Sec. II B. The value of $G_{D,q}$, for charged defects, includes the first order multipole correction described in Sec. II B. The third term represents the free energy term due to the loss of n_i atoms of type i that occurs when the defect is formed (a negative value of n_i denotes addition of atoms). The fourth term represents the free energy change due to exchange of electrons and holes with the carrier reservoirs. ΔE_v is the electrostatic potential alignment correction, which represents the offset between the VBM in the neutral and charged systems. Finally, E_F is the Fermi energy relative to the VBM, which is bound between the VBM and the CBM.

E. Electronic transition energies

The transition energy $\varepsilon(D,q/q')$ is defined as the Fermi energy at which the charge state of defect D spontaneously transforms $q \leftrightarrow q'$. Therefore, at $E_F = \varepsilon(D,q/q')$ the formation energies of both defects are the same: $\Delta G_{D,q}(E_F,\mu) = \Delta G_{D,q'}(E_F,\mu)$. Using Eq. (11) the transition energy can be expressed as:

$$\varepsilon(D,q/q') = \frac{G_{D,q} - G_{D,q'}}{(q' - q)} - \Delta E_v. \quad (12)$$

F. Defect concentration

At equilibrium the defect concentration obeys Boltzmann statistics and so it is given by

Downloaded 02 Feb 2011 to 155.198.39.40. Redistribution subject to AIP license or copyright; see http://jap.aip.org/about/rights_and_permissions

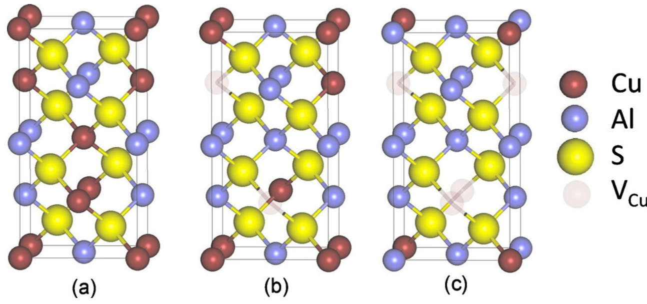

FIG. 1. (Color online) The (16 atom) conventional unit cell of $CuAlS_2$ is shown. (a) indicates the $CuAlS_2$ crystalline structure. (b) shows the $2V_{Cu}^{1-}+Al_{Cu}^{2+}$ defect in $CuAlS_2$ and figure (c) indicates the crystalline structure of $CuAl_5S_8$.

$$c_{D,q}(E_F,\mu_i,T) = N \exp[-\Delta G_{D,q}(E_F,\mu)/k_B T], \quad (13)$$

where N is the total number of atomic sites where the defect can occur, k_B is the Boltzmann constant, and T is temperature. The condition that the overall system must remain charge neutral enables E_F to be determined self consistently. The neutrality condition is given by

$$\sum_D q_D c_D = 0, \quad (14)$$

where q_D is the charge of defect D and c_D is the concentration of the defect.

G. ODCs

The procedure Zhang *et al.*[15] applied to $CuInSe_2$ was used to construct the unit cells for $CuAl_5S_8$ and $CuAl_3S_5$. The method involves creating compound defects in $CuAlS_2$ supercells. For instance, $CuAl_5S_8$ is obtained by creating a $(2V_{Cu}^{1-}+Al_{Cu}^{2+})^0$ compound defect in a 16 atom $CuAlS_2$ supercell. Figure 1 shows an schematic picture of $CuAl_5S_8$.

III. RESULTS

A. $CuAlS_2$ bulk

The computed and experimental lattice parameters are given in Table II. The lattice parameters are overestimated by around 2% for $CuAlS_2$, which is typical for B3LYP calculations on wide bandgap insulators. The calculated density of states for $CuAlS_2$ is shown in Fig. 2. The calculated band gap is 3.5 eV, which is in agreement with the experimental values measured for the optical band gap of $CuAlS_2$: 3.55 eV (Ref. 6) and 3.5 eV.[38]

B. Phase stability

Figure 3 is the computed phase diagram as a function of the aluminum and copper chemical potentials. It was calculated as explained in Sec. II C and highlights the stability region for $CuAlS_2$. This figure is a phase diagram projected in the $(\Delta\mu_{Cu},\Delta\mu_{Al})$ plane. $\Delta\mu_S$ is constrained by Eq. (3), and the diagonal line which links the $\Delta\mu_{Cu}$ and $\Delta\mu_{Al}$ axes represents $\Delta\mu_S$=0 eV. Points 1–2-3–4 indicate the corners of the stability region. The strip region stretching parallel to the line defined by points 1 and 4 indicates the stability region for the $CuAl_5S_8$ ODC.

TABLE II. Calculated lattice constants for $CuAlS_2$. The experimental values (Ref. 1) are given in parenthesis.

	a (Å)	*c* (Å)	*a*/*c*
$CuAlS_2$	5.47 (5.32)	10.55 (10.43)	1.93 (1.96)

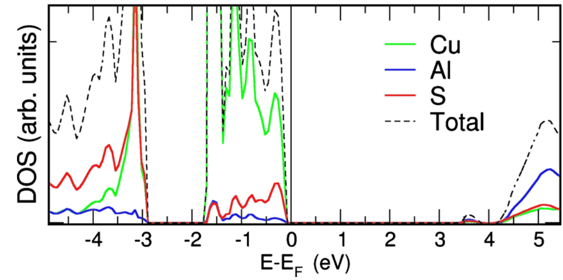

FIG. 2. (Color online) Projected density of states for bulk $CuAlS_2$. The Fermi energy is the zero of energy.

C. Defect energies

The formation energies of the calculated defects along the boundary of the $CuAlS_2$ stability region are shown in Fig. 4. The formation energies of all the defects studied are depicted: The copper and sulfur vacancies $V_{Cu}^{0/1+/2+}$ and $V_S^{1-/0}$; the copper substituting aluminum $Cu_{Al}^{2-/1-/0}$; the aluminum substituting copper $Al_{Cu}^{0/1+/2+}$; and the compound $(2V_{Cu}^{1-}+Al_{Cu}^{2+})^0$ defect. The equilibrium defect concentration is calculated using Eq. (13), and the temperature adopted is 900 K, which is a typical temperature for the growth of $CuAlS_2$.[4,5] The defect concentrations depend explicitly on the equilibrium Fermi energy, E_F, through the defect formation energies and, in turn, E_F depends on the concentration of the charged defects through the neutrality condition expressed in Eq. (14). Therefore, the values of the defects concentrations and E_F are determined self consistently.

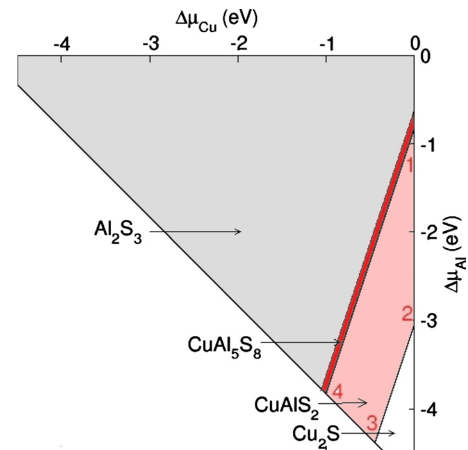

FIG. 3. (Color online) Calculated phase diagram for the Cu–Al–S system indicating the stable phases in the vicinity of $CuAlS_2$. $\Delta\mu_{Cu}$=0 and $\Delta\mu_{Al}$ =0 indicates Cu-rich, Al-rich regions. Since $\Delta\mu_S$ is defined through Eq. (2), the $\Delta\mu_{Cu}$=$\Delta\mu_{Al}$=0 also indicates a S-poor region. The diagonal line which links the $\Delta\mu_{Cu}$ and $\Delta\mu_{Al}$ axes represents a sulfur rich region with $\Delta\mu_S$=0.

Downloaded 02 Feb 2011 to 155.198.39.40. Redistribution subject to AIP license or copyright; see http://jap.aip.org/about/rights_and_permissions

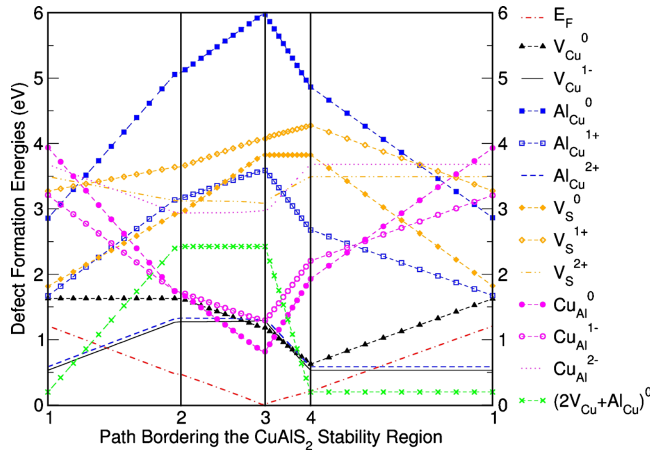

FIG. 4. (Color online) Defect formation energies at the border of the $CuAlS_2$ stability region. This region is defined by the lines connecting the points 1–2–3–4 in Fig. 3.

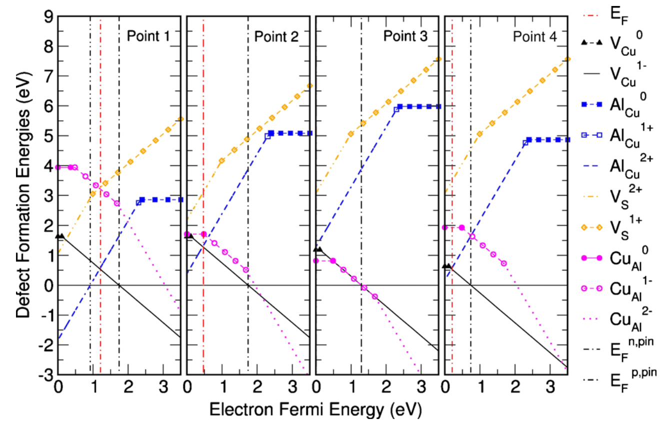

FIG. 5. (Color online) Defect formation energies at the four corners of the stability region of $CuAlS_2$ (Fig. 3). At these four points, labeled 1, 2, 3, and 4, the chemical potentials μ_i have fixed values, and the defect formation energy is a function of the Fermi energy, whose values range have been assumed to be vary from the VBM up to the CBM. The breaking points of each line indicate the transition energies between different charged states of the defect. In each plot, vertical dashed-dotted lines mark the *n* and *p*-type doping limits, and a red dashed-dotted line indicates the equilibrium Fermi energy E_F, which has been calculated self-consistently using the neutrality condition [Eq. (3)] at a temperature of 900 K.

Along lines 1–2 and 4–1, and part of line 2–3, the point defects with the lowest formation energies are V_{Cu}^{1-} and Al_{Cu}^{2+}. Along the remainder of line 2–3 the Cu_{Al}^{0} defect dominates, having its minimum formation energy at point 3. Finally, along line 3–4 the most stable point defects are Cu_{Al}^{0}, V_{Cu}^{0}, V_{Cu}^{1-}, and Al_{Cu}^{2+}. The formation energy of the compound defect $(2V_{Cu}^{1-}+Al_{Cu}^{2+})^0$ is also plotted in Fig. 4: This defect is comprised of point defects V_{Cu}^{1-} and Al_{Cu}^{2+}. The interaction energy of the compound defect, ΔE_{int}, is defined as:

$$\Delta E_{int} = E[(2V_{Cu}^{1-} + Al_{Cu}^{2+})^0] - 2E(V_{Cu}^{1-}) - E(Al_{Cu}^{2+}). \quad (15)$$

At all points along the path bordering the stability region of $CuAlS_2$ ΔE_{int} has a value of -1.45 eV, which is independent of $\Delta\mu_i$ and E_F. Point defects V_{Cu}^{1-} and Al_{Cu}^{2+} are, hence, stabilized by the formation of the $(2V_{Cu}^{1-}+Al_{Cu}^{2+})^0$ compound defect. This implies that at high concentrations of V_{Cu}^{1-} and Al_{Cu}^{2+}, their energies are further lowered by interactions with nearby defects. The $(2V_{Cu}^{1-}+Al_{Cu}^{2+})^0$ compound defects are most stable along the line 1–4. This is expected as this line represents the region in which $CuAlS_2$ is at equilibrium with the $CuAl_5S_8$ ODC, which consists of ordered arrangements of the $(2V_{Cu}^{1-}+Al_{Cu}^{2+})^0$ compound defect.

Figure 5 shows the defect formation energies of the point defects at the four corners of the stability region of $CuAlS_2$. At each of these four points, the chemical potentials have fixed values and, therefore, the formation energy given by Eq. (11) is only a function of E_F, and can be written as:

$$\Delta G_{D,q}(E_F) = K_D + qE_F, \quad (16)$$

where K_D is a constant characteristic of each defect.

Figure 5 may be used to analyze the possibility of type-inversion[39] in $CuAlS_2$. In principle, any semiconductor can be either *n* or *p*-doped. In practice, however, semiconductor dopability is limited. For instance, ZnO and ZnS are *n*-type semiconductors that cannot be made *p*-type,[40] and $CuAlSe_2$ is a *p*-type semiconductor that cannot be made *n*-type.[41] Doping limits exist because doping with donors (acceptors) moves the equilibrium Fermi energy toward the CBM (VBM). In this way, the formation energy of acceptors (donors) is lowered, and is easier for the acceptors (donors) to form spontaneously. This mechanism compensates the intentional donor (acceptor) dopants, and leads to the pinning of the Fermi energy at an energy we label as $E_F^{n,pin}$ ($E_F^{p,pin}$). This mechanism can be understood from an examination of Eq. (16).

Ideally, for a system to become *n*-type, $E_F^{n,pin}$ should be as high in the band gap as possible, even inside the conduction band. Figure 5 shows that, at points 1, 2, 3, and 4 the maximum value for $E_F^{n,pin}$ is less than half of the band gap energy. Conversely, $E_F^{p,pin}$ is ≈ 1 eV above the VBM at point 1 and below the VBM at all the other points.

The position of E_F in the band gap (E_G) determines the type of doping: if $E_F \geq VBM+(E_G/2)$, the system is *n*-type; if $E_F \leq VBM+(E_G/2)$, the system is *p*-type. In Fig. 4 the value of E_F is always smaller than half the band gap, which indicates that $CuAlS_2$ is a *p*-type material under these environmental conditions, a prediction that agrees with experimental evidence.[4]

D. Electronic transition energies

Table III and Fig. 6 show the transition energies calculated using Eq. (12). V_{Cu} and Cu_{Al} defects both contribute acceptor levels while Al_{Cu} defects contribute donor levels. As regards V_S defects, they are expected to form donor levels, as one or two electrons are donated to the system when V_S^{1+} and V_S^{0} are formed. In the case of $CuAlS_2$, it has been suggested that these electrons *n*-dope the system.[6,10] Experimental measurements on $CuGaSe_2$ and $CuInSe_2$ have shown, however, that V_{Se} defects could cause persistent hole photoconductivity (*p*-type persistent photo-conductivity (PPC)).[42] This is because the two electrons left behind by the neutral Se vacancy form a defect localized state that lies at energies below the VBM. Therefore, optical excitement of the V_{Se}^{2+} defect initiates the reaction $V_{Se}^{2+} \rightarrow V_{Se}^{0}+2h$, which traps two electrons, releasing two holes to the valence band. Similarly,

Downloaded 02 Feb 2011 to 155.198.39.40. Redistribution subject to AIP license or copyright; see http://jap.aip.org/about/rights_and_permissions

TABLE III. Calculated transition energies of vacancies and substitutional defects as defined by Eq. (12). The corresponding charge states for these transitions are given in parentheses. The transition energies are relative to the VBM for acceptors and to the CBM for donors. The transition energy (0/1+) in V_S is below the VBM.

Defect	(q/q′)	ε(D,q/q′) (eV)
V_{Cu}	(1−/0)	0.11
Al_{Cu}	(0/1+)	1.10
Al_{Cu}	(1+/2+)	1.20
Cu_{Al}	(2−/1−)	1.68
Cu_{Al}	(1−/0)	0.48
V_S	(0/1+)	−0.24
V_S	(1+/2+)	0.99

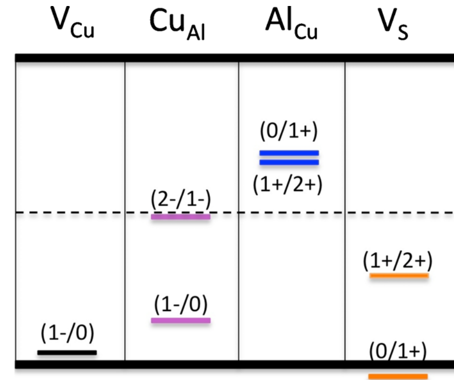

FIG. 6. (Color online) Calculated defect transition energies as defined by Eq. (12). Their precise values are given in Table III. The transitional charge states are indicated in parenthesis. The thick black lines at the top and bottom represent the CBM and VBM respectively.

V_{Se}^{1+} releases one hole to the acceptor level. To the best of the authors knowledge, there are no experimental data suggesting that PPC occurs in $CuAlS_2$. However, Fig. 6 shows the transition energies associated with V_S, and it can be clearly seen that the (0/1+) transition state lies below the VBM, and that the (1+/2+) transition state lies below the middle of the band gap. These results suggest that V_S is behaving as an acceptor and could potentially *p*-dope the system.

PL measurements carried out by Chichibu *et al.*[4] on low-grade $CuAlS_2$ defective samples showed three shallow acceptor levels at 0.08, 0.175, and 0.250. They did not specify the growing conditions and did not assign any of these levels to any particular defect. Moreover, inductively coupled plasma spectroscopy found that $CuAlS_2$ single crystals, grown by the chemical vapor transport technique, are copper deficient.[43] Electron spin resonance (ESR) and thermal quenching measurements on these samples identified an isotropic signal. This ESR signal was linked to a copper vacancy, whose associated defect level had an ionization energy of $E_A = 0.190 \pm 0.01$ eV.[43] This conclusion is in agreement with the data presented here (Fig. 4) which suggest that V_{Cu} is the most stable defect at most points along the phase stability region.

E. PL in defective $CuAlS_2$

A wide variety of processes have been suggested as interpretation of the observed PL emissions that are listed in Table IV, these include:

- FE recombination.
- Radiative recombination of a free hole and a donor ($h\mathbb{D}^0$).
- Radiative recombination of a free electron and an acceptor (free-to-bound emission) ($e\mathbb{A}^0$).
- Excitonic emission bound to a neutral acceptor ($\mathbb{A}^0X$).
- Excitonic emission bound to a singly-charged acceptor ($\mathbb{A}^-X$).
- Excitonic emission bound to a neutral donor ($\mathbb{D}^0X$).
- Excitonic emission bound to a singly-charged donor ($\mathbb{D}^+X$).
- Donor acceptor pair recombination ($\mathbb{D}^+\mathbb{A}^-$).

It is suggested, from our calculations, that $\mathbb{D}$ is Al_{Cu}, and $\mathbb{A}$ is either V_{Cu}, V_S, or Cu_{Al}. Since the data is insufficient to unambiguously associate the observed PL emissions with specific defects, the experiments need to be complemented with theoretical data, such as the calculated energy of the PL emissions associated with each of the studied defects. The energy of a PL emission is given by:

$$h\nu = E_G - E_{BE}, \quad (17)$$

where $E_G = 3.5$ eV is the calculated band gap and E_{BE} is the binding energy associated with the given emission. The E_{BE} for a FE recombination is R_x. In PL emissions associated with the radiative recombination of a free hole and a donor ($h\mathbb{D}^0$), or a free electron and an acceptor ($e\mathbb{A}^0$), E_{BE} can be estimated as the electronic transition energies $\varepsilon(\mathbb{D},q/q')$ or $\varepsilon(\mathbb{A},q/q')$, respectively. If excitons are bound to neutral and ionized donors or acceptors the value of E_{BE}, although still dependent on $\varepsilon(\mathbb{D},q/q')$ or $\varepsilon(\mathbb{A},q/q')$, is modified. For instance, PL experiments on II-IV compounds yielded PL emissions that were interpreted as resulting from an exciton-neutral-defect complex.[44–46] These results showed that the E_{BE} of the exciton-neutral-defect complex is about 0.20 times the E_{BE} of the corresponding radiative recombination process of the associated defect [$E_{BE} = 0.20\varepsilon(\mathbb{D},q/q')$]. Sharma and Rodriguez[47] and Atzmüller *et al.*[48] estimated E_{BE} for bound excitons as a function of the ratio between the effective masses of the electrons and holes: $s = m_e^*/m_h^*$. In this work the ratio between effective masses m_e^* and m_h^* has been calculated at the Γ point as: $s = m_e^*/m_h^* = (\partial^2 E_{VB}(k)/\partial k^2)_\Gamma / (\partial^2 E_{CB}(k)/\partial k^2)_\Gamma$, where the second order derivatives have been calculated along the $(-100) \to (000) \to (100)$, $(0-10) \to (000) \to (010)$ and $(00-1) \to (000) \to (001)$ directions in the reciprocal space. The calculated average values of the electron and holes effective masses are $\hbar^2 0.26$ and $\hbar^2 1.58$, respectively, and the value adopted for s in $CuAlS_2$ is $s = 0.165$. Using the calculated values for the effective masses we have also estimated the reduced mass of the electron-hole pair and, with it, the value of binding energy for the FE: $R_x = 62$ meV. Within the model proposed by Sharma and Rodriguez, the expressions for calculating the energy of the PL emissions associated with defect-bound excitons in $CuAlS_2$ are:

$$E_{BE} = R_x + 1.00\varepsilon(\mathbb{D},0/1+) \quad \text{for } (\mathbb{D}^+X), \quad (18)$$

Downloaded 02 Feb 2011 to 155.198.39.40. Redistribution subject to AIP license or copyright; see http://jap.aip.org/about/rights_and_permissions

TABLE IV. Observed PL emissions on $CuAlS_2$ samples. The synthesis methods are indicated in the second column. The temperature at which the PL emission was observed and its corresponding intensity and FWHM are indicated in the third and fourth columns. Columns five and six show the proposed experimental and theoretical origins of the observed PL emissions: (A) FE recombination; ($\mathbb{D}^0$X) excitonic emission bound to a neutral donor; ($\mathbb{D}^+$X) excitonic emission bound to a singly-charged donor; (h$\mathbb{D}^0$) radiative recombination of a free hole and a donor; ($\mathbb{A}^0$X) excitonic emission bound to a neutral acceptor; ($\mathbb{A}^-$X) excitonic emission bound to a singly-charged acceptor; (e$\mathbb{A}^0$) radiative recombination of a free electron and an acceptor (free-to-bound emission); and ($\mathbb{D}^+\mathbb{A}^-$) is a donor acceptor pair recombination. The subscript s indicates a strong PL intensity.

Refs.	Sample preparation and quality	Temp. (K)	PL emissions (FWHM) (eV)	Exp. PL origin	Theo. PL origin
Chichibu *et al.*[4]	LP-MOVPE, high grade	10	3.52_s (0.1), 2.76 (0.4)	A, ($\mathbb{A}^0$X) or ($\mathbb{A}^-$X)	A, ($\mathbb{D}^+\mathbb{A}^-$)
Chichibu *et al.*[4]	LP-MOVPE, low grade	10	3.43 (0.1), 3.34_s (0.1), 2.76 (0.4)	(e$\mathbb{A}^0$), (e$\mathbb{A}^0$), ($\mathbb{A}^0$X) or ($\mathbb{A}^-$X)	(e$\mathbb{A}^0$), (e$\mathbb{A}^0$), ($\mathbb{D}^+\mathbb{A}^-$)
Kuroki *et al.*[6,12]	Pellets ann. at 1073, defective K	298	1.90_s (0.3)	($\mathbb{D}^+\mathbb{A}^-$)	($\mathbb{D}^+\mathbb{A}^-$)
Kuroki *et al.*[6,12]	Pellets ann. at 1123 K, defective	298	1.90_s (0.3)	($\mathbb{D}^+\mathbb{A}^-$)	($\mathbb{D}^+\mathbb{A}^-$)
Kuroki *et al.*[6,12]	Pellets ann. at 937 K, defective+CuS	15, 30, 50, 70	3.55 (0.05), 2.10 (0.4)	A, ($\mathbb{D}^+\mathbb{A}^-$)	A, ($\mathbb{D}^+\mathbb{A}^-$)
Kuroki *et al.*[6,12]	Pellets, ann. at 937 K, defective+CuS	15, 30, 50, 70	3.45 (0.05), 2.10 (0.4)	($\mathbb{D}^0$X) or (h$\mathbb{D}^0$), ($\mathbb{D}^+\mathbb{A}^-$)	($\mathbb{D}^0$X), ($\mathbb{D}^+\mathbb{A}^-$)
Shikarata *et al.*[5]	CVT, stoichiometric mix., defective	10	3.55 (0.05), 2.1_s (0.3)	A, N/A	A, ($\mathbb{D}^+\mathbb{A}^-$)
Shikarata *et al.*[5]	CVT, Cu rich, defective	10	3.55 (0.05), 3.0_s (0.1)	A, N/A	A, (e$\mathbb{A}^0$)
Shikarata *et al.*[5]	CVT, Al rich, defective	10	3.55 (0.05), 2.1_s (0.3)	A, N/A	A, ($\mathbb{D}^+\mathbb{A}^-$)

$$E_{BE} = R_x + 1.18\varepsilon(\mathbb{A},1-/0) \quad \text{for } (\mathbb{A}^-X), \tag{19}$$

$$E_{BE} = R_x + 0.29\varepsilon(\mathbb{D},0/1+) \quad \text{for } (\mathbb{D}^0X), \tag{20}$$

$$E_{BE} = R_x + 0.11\varepsilon(\mathbb{A},0/1+) \quad \text{for } (\mathbb{A}^0X), \tag{21}$$

where $\varepsilon(\mathbb{D}\text{or}\mathbb{A},q/q')$ is the activation energy of the donor or acceptor involved in the process. Finally, E_{BE} for PL emissions associated with ($\mathbb{D}^+\mathbb{A}^-$) transitions is given by:[49]

$$E_{BE} = [\varepsilon(\mathbb{D},q/q') + \varepsilon(\mathbb{A},q/q')] + \frac{e^2}{\varepsilon r} + C(r). \tag{22}$$

The E_{BE} of a ($\mathbb{D}^+\mathbb{A}^-$) transition depends on the distance r between the two defects. e^2/ε_r is a Coulomb contribution and C(r) is a correction used for small values of r. C(r) tends to zero when r tends to infinity. In Table V the calculated PL emissions are summarized. The PL emissions associated with ($\mathbb{D}^+\mathbb{A}^-$) have been estimated at C(r)=0, an assumption that will be discussed later.

To simplify the comparison between experimental and theoretical results, the PL emissions observed by Kuroki and co-workers,[6,12] Shirakata *et al.*,[5] and Chichibu *et al.*[4] are classified into three sets: (a) FE PL emissions of 3.52 (Ref. 4) and 3.55 eV;[6,12] (b) NBEPL emissions of 3.34, 3.43,[4] 3.0 eV,[5] and emissions at 3.45 eV;[12] and (c) mid-band gap emissions of 1.90,[6,12] 2.76,[4] and 2.10 eV.[5]

The calculated FE emission is 3.44 eV (Table V). This result suggests that the observed emissions of 3.55 and 3.52 eV [with a full width at half maximum (FWHM) of 0.05 eV] are due to FE emissions. The NBEPL emissions of 3.43 and 3.34 eV were observed in samples known to be *p*-type and their intensities were linearly proportional to the power of the exciting laser radiation, which helped with identifying the underlying recombination process of the NBEPL emisions.[4,47] These emissions where therefore assumed to be due to free-to-bound type transitions related to an acceptor. The free-to-bound transition 8 (Table V) has a PL emission of 3.39 eV and involves the V_{Cu} acceptor, which is the most stable intrinsic defect in $CuAlS_2$ under a wide range of environmental conditions (Fig. 4). It is therefore concluded that either of the observed 3.43 and 3.34 eV PL emissions is due to emission 8. Since the FWHM of the observed emissions is 0.1 eV, it is not possible to determine specifically which of the two emissions is related with V_{Cu}. The other two NBEPL emissions of 3.45 eV and 3.00 eV were observed on samples grown under stoichiometric[4,6,12] and Cu-rich conditions,[5] respectively. The origin of these PL emissions was not concluded from these experiments. On the basis of the calculated PL emissions and thermodynamic stability, emission 6 (3.44 eV) in Table V might be the origin of the 3.45 eV NBEPL emission. Emission 6 is also related with V_{Cu}. The

TABLE V. Calculated values of the PL emission energies, $h\nu_{CAL}$, associated with different defect states in $CuAlS_2$. E_G=3.5 eV is the calculated band gap and R_x=0.07 eV is the FE binding energy. The second column shows the form Eq. (17) adopt depending on the type of PL emission and the defects involved. The values of the electronic transition energies $\varepsilon(\text{DorA},q/q')$ used on the expressions on the second column were taken from Table III.

Identifier	Type	Expression for PL emission	$h\nu_{CAL}$ (eV)
1	FE	$E_G - R_x$	3.44
2	$I_{\mathbb{D}^0X}$	$E_G - 0.29\varepsilon(Al_{Cu},0/1+) - R_x$	3.12
3	$I_{\mathbb{D}^+X}$	$E_G - 1.00\varepsilon(Al_{Cu},0/1+) - R_x$	2.34
4	$I_{h\mathbb{D}^0}$	$E_G - \varepsilon(Al_{Cu},0/1+)$	2.40
5	$I_{h\mathbb{D}^0}$	$E_G - \varepsilon(Al_{Cu},1+/2+)$	2.30
6	$I_{\mathbb{A}^0X}$	$E_G - 0.11\varepsilon(V_{Cu},1-/0) - R_x$	3.44
7	$I_{\mathbb{A}^-X}$	$E_G - 1.18\varepsilon(V_{Cu},1-/0) - R_x$	3.31
8	$I_{e\mathbb{A}^0}$	$E_G - \varepsilon(V_{Cu},1-/0)$	3.39
9	$I_{\mathbb{A}^0X}$	$E_G - 0.11\varepsilon(Cu_{Al},1-/0) - R_x$	3.39
10	$I_{\mathbb{A}^-X}$	$E_G - 1.18\varepsilon(Cu_{Al},1-/0) - R_x$	2.87
11	$I_{e\mathbb{A}^0}$	$E_G - \varepsilon(Cu_{Al},2-/1-)$	1.82
12	$I_{e\mathbb{A}^0}$	$E_G - \varepsilon(Cu_{Al},1-/0)$	3.02
13	$I_{e\mathbb{A}^0}$	$E_G - \varepsilon(V_S,0/1+)$	3.74
14	$I_{e\mathbb{A}^0}$	$E_G - \varepsilon(V_S,1+/2+)$	2.51
15	$I_{\mathbb{D}^+\mathbb{A}^-}$	$E_G - [\varepsilon(Al_{Cu},0/1+) + \varepsilon(V_{Cu},1-/0)]$	2.29
16	$I_{\mathbb{D}^+\mathbb{A}^-}$	$E_G - [\varepsilon(Al_{Cu},0/1+) + \varepsilon(Cu_{Al},1-/0)]$	1.92
17	$I_{\mathbb{D}^+\mathbb{A}^-}$	$E_G - [\varepsilon(Al_{Cu},0/1+) + \varepsilon(Cu_{Al},2-/1-)]$	0.72
18	$I_{\mathbb{D}^+\mathbb{A}^-}$	$E_G - [\varepsilon(Al_{Cu},0/1+) + \varepsilon(V_S,1+/2+)]$	1.41
19	$I_{\mathbb{D}^+\mathbb{A}^-}$	$E_G - [\varepsilon(Al_{Cu},1+/2+) + \varepsilon(V_{Cu},1-/0)]$	2.19
20	$I_{\mathbb{D}^+\mathbb{A}^-}$	$E_G - [\varepsilon(Al_{Cu},1+/2+) + \varepsilon(Cu_{Al},1-/0)]$	1.82
21	$I_{\mathbb{D}^+\mathbb{A}^-}$	$E_G - [\varepsilon(Al_{Cu},1+/2+) + \varepsilon(Cu_{Al},2-/1-)]$	0.62
22	$I_{\mathbb{D}^+\mathbb{A}^-}$	$E_G - [\varepsilon(Al_{Cu},1+/2+) + \varepsilon(V_S,1+/2+)]$	1.31

Downloaded 02 Feb 2011 to 155.198.39.40. Redistribution subject to AIP license or copyright; see http://jap.aip.org/about/rights_and_permissions

calculated PL emissions and thermodynamic stability suggest the 3.0 eV NBEPL emission can be assigned to emission 12 (3.02 eV) on Table V. This emission is linked with Cu_{Al} which is stabilized under Cu-rich conditions.

The 2.76, 2.10, and 1.90 eV mid-band gap emissions are broad-peak emissions. The 2.76 eV emission has been observed in *p*-type systems but, for the other two emissions, there is no information available on whether the samples are *p* or *n*-type doped or on the nature of the defect causing the PL emission. Low temperature broad emissions are generally linked with $(\mathbb{D}^{+}\mathbb{A}^{-})$ type transitions: As the defect concentration increases, the Coulomb-type term in Eq. (22) increases as the distance between distant defect pairs is reduced, resulting in a broad emission band.[49] It is shown in Fig. 4 that the $(\mathbb{D}^{+}\mathbb{A}^{-})$ pair formed by V_{Cu}^{1-} and Al_{Cu}^{2+} is stable. Moreover when the concentration of these defects is large enough, the interaction between them leads to the formation of the $CuAl_5S_8$ ODC, and it is assumed this renders the C(r) term in Eq. (22) as negligible.[50] The 1.90 eV and 2.10 eV emissions were observed in samples annealed at 1073 K and 1123 K,[6,12] respectively, and in Al-rich $Cu_{0.97}Al_{1.03}S_2$ samples.[5] The stable pair formed by V_{Cu}^{1-} and Al_{Cu}^{2+} defects is likely to have been formed under these conditions, and transition 19 in Table V indicates it has an associated PL emission of 2.19 eV, which will be broadened by the interaction of distant defect pairs. Therefore, the combined experimental and theoretical evidence suggests that the $(\mathbb{D}^{+}\mathbb{A}^{-})$ pair as being responsible for the 2.10 and 1.90 eV broad emissions. The 2.76 eV emission has been experimentally linked with a bound-to-free (BF) transition involving a deep acceptor whose thermal quenching process was dominated by nonradiative recombination centers.[4] Although the theoretical results suggest PL emissions, that are associated with deep acceptor levels, occur at values that are comparable with experiments (for instance, emission 10 in Table V: 2.87 eV), none of these can account for the broadness of the experimentally observed PL emission. Therefore, the experimentally proposed BF transition has to coexist with a $(\mathbb{D}^{+}\mathbb{A}^{-})$ transition. The theoretical results suggest the $(\mathbb{D}^{+}\mathbb{A}^{-})$ transition has to be between the pair formed by the V_{Cu}^{1-} and Al_{Cu}^{2+} defects.

IV. CONCLUSIONS

Ab initio thermodynamics has been used to study the thermodynamic stability of $CuAlS_2$ and its intrinsic defects. It has been shown that the $CuAlS_2$ is a *p*-type material, and that depending on the environmental conditions, the compound defect $(2V_{Cu}^{1-}+Al_{Cu}^{2+})^0$ has the lowest formation energy of all the defects considered. This is consistent with the stability of the predicted $CuAl_5S_8$ ODC, which originates from a high concentration of this type of compound defect.

In addition, our results suggest that $CuAlS_2$ broad visible PL emission, centered at around 2 eV, is due to radiative recombinations that occur between the band gap states related to the Al_{Cu}^{2+} and V_{Cu}^{1-} defects. As regards the room-temperature ultraviolet emission, our results match and complement current experimental evidence, suggesting that UV emissions are related with: (a) FE emissions in nondefective $CuAlS_2$; and (b) NBEPL emissions connected with V_{Cu} and Cu_{Al} defects.

ACKNOWLEDGMENTS

The calculations performed for this work were carried out in part on the facilities of Imperial College High Performance Computing Service (URL: http://www.imperial.ac.uk/ict/services/teachingandresearchservices/highperformancecomputing), and in part on the national high-performance computing service of the UK, HECToR, where computer time has been provided via our membership of the HPC Materials Chemistry Consortium of the UK and funded by the EPSRC (portfolio Grant No. EP/F067496).

This work was funded by the EPSRC under the "Nanostructured Functional Materials for Energy Efficient Refrigeration, Energy Harvesting, and Production of Hydrogen from Water" grant (Grant No. EP/G060940/1).

[1] J. E. Jaffe and A. Zunger, Phys. Rev. B **28**, 5822 (1983).
[2] K. Sato, K. Ishii, K. Watanabe, and K. Ohe, Jpn. J. Appl. Phys., Part 1 **30**, 307 (1991).
[3] M. L. Liu, F. Q. Huang, L. D. Chen, Y. M. Wang, Y. H. Wang, G. F. Li, and Q. Zhang, Appl. Phys. Lett. **90**, 072109 (2007).
[4] S. Chichibu, S. Shirakata, S. Isomura, and H. Nakanishi, Jpn. J. Appl. Phys., Part 1 **36**, 1703 (1997).
[5] S. Shirakata, I. Aksenov, K. Sato, and S. Isomura, Jpn. J. Appl. Phys., Part 2 **31**, L1071 (1992).
[6] Y. Kuroki, T. Okamoto, M. Takata, and M. Osada, Appl. Phys. Lett. **89**, 221117 (2006).
[7] Y. Chen, D. M. Bagnall, H. J. Koh, K. T. Park, K. Hiraga, Z. Zhu, and T. Yao, J. Appl. Phys. **84**, 3912 (1998).
[8] I. Aksenov and K. Sato, Appl. Phys. Lett. **61**, 1063 (1992).
[9] I. Aksenov and K. Sato, Jpn. J. Appl. Phys., Part 1 **31**, 2352 (1992).
[10] I. Aksenov, N. Nishikawa, and K. Sato, J. Appl. Phys. **74**, 3811 (1993).
[11] K. Sato, in *Japanese Research Review for Pioneering Ternary and Multinary Compounds in the 21st Century*, edited by S. S. S. T. W. T. Matsuzawa, T. Takizawa, and N. Yamamoto (The Institute of Pure and Applied Physics, Tokyo, 2001), p. 228.
[12] Y. Kuroki, A. Kato, T. Okamoto, and M. Takata, J. Electroceram. **21**, 378 (2008).
[13] J. Cáceres and C. Rincón, Phys. Status Solidi B **234**, 541 (2002).
[14] C. Rincón, S. M. Wasim, and G. Marín, Appl. Phys. Lett. **80**, 998 (2002).
[15] S. B. Zhang, S. H. Wei, A. Zunger, and H. Katayama-Yoshida, Phys. Rev. B **57**, 9642 (1998).
[16] T. J. Coutts, L. L. Kazmerski, and S. Wagner, *Copper Indium Diselenide for Photovoltaic Applications* (Elsevier Science, New York, NY, 1986).
[17] J. Vidal, S. Botti, P. Olsson, J.-F. Guillemoles, and L. Reining, Phys. Rev. Lett. **104**, 056401 (2010).
[18] S. B. Zhang, S. H. Wei, and A. Zunger, Phys. Rev. Lett. **78**, 4059 (1997).
[19] M. Grossberg, J. Krustok, I. Bodnar, S. Siebentritt, and J. Albert, Physica B **403**, 184 (2008).
[20] R. Dovesi, V. R. Saunders, C. Roetti, R. Orlando, C. M. Zicovich-Wilson, F. Pascale, B. Civalleri, K. Doll, N. M. Harrison, I. J. Bush, P. D'Arco, and M. Llunell, *CRYSTAL 2006 User's Manual* (University of Torino, Italy, 2007).
[21] P. J. Stephens, F. J. Devlin, C. F. Chabalowski, and M. J. Frisch, J. Phys. Chem. **98**, 11623 (1994).
[22] A. D. Becke, J. Chem. Phys. **98**, 1372 (1993).
[23] J. Muscat, A. Wander, and N. M. Harrison, Chem. Phys. Lett. **342**, 397 (2001).
[24] S. Tomić, B. Montanari, and N. M. Harrison, Physica E **40**, 2125 (2008).
[25] J. Heyd, J. Peralta, G. Scuseria, and R. Martin, J. Chem. Phys. **123**, 174101 (2005).
[26] See supplementary material at http://dx.doi.org/10.1063/1.3544206 for description of the basis sets.
[27] P. Ewald, Ann. Phys. **369**, 253 (1921).
[28] C. G. Van de Walle and J. Neugebauer, J. Appl. Phys. **95**, 3851 (2004).
[29] G. Makov and M. C. Payne, Phys. Rev. B **51**, 4014 (1995).

Downloaded 02 Feb 2011 to 155.198.39.40. Redistribution subject to AIP license or copyright; see http://jap.aip.org/about/rights_and_permissions

[30]C. L. Bailey, L. M. Liborio, G. Mallia, S. Tomić, and N. M. Harrison, Phys. Rev. B **81**, 205214 (2010).
[31]P. Lukashev, W. R. L. Lambrecht, T. Kotani, and M. van Schilfgaarde, Phys. Rev. B **76**, 195202 (2007).
[32]E. E. Hellstrom and R. A. Huggins, Mater. Res. Bull. **14**, 127 (1979).
[33]K. Reuter and M. Scheffler, Phys. Rev. B **65**, 035406 (2001).
[34]K. Reuter and M. Scheffler, Phys. Rev. B **68**, 045407 (2003).
[35]K. Reuter and M. Scheffler, Phys. Rev. Lett. **90**, 046103 (2003).
[36]B. Korzun, R. Mianzelen, A. Sheleg, N. Tekhanovich, K. Bente, and W. Schmitz, Phys. Status Solidi B **242**, 1990 (2005).
[37]B. Eckert and R. Steudel, Top. Curr. Chem. **231**, 31 (2003).
[38]R. Bhandari, Y. Hashimoto, and K. Ito, Jpn. J. Appl. Phys., Part 1 **43**, 6890 (2004).
[39]U. Rau, K. Taretto, and S. Siebentritt, Appl. Phys. A: Mater. Sci. Process. **96**, 221 (2009).
[40]J. Hu and R. Gordon, J. Appl. Phys. **72**, 5381 (1992).
[41]B. Tell, J. Shay, and H. Kasper, J. Appl. Phys. **43**, 2469 (1972).
[42]S. Lany and A. Zunger, Phys. Rev. B **72**, 035215 (2005).
[43]Y. S. I. Aksenov, T. Yasuda, and K. Sato, J. Appl. Phys. **74**, 2106 (1993).
[44]J. Haynes, Phys. Rev. Lett. **4**, 361 (1960).
[45]R. Halsted and M. Aven, Phys. Rev. Lett. **14**, 64 (1965).
[46]Y. S. Park, C. W. Litton, T. C. Collins, and D. C. Reynolds, Phys. Rev. **143**, 512 (1966).
[47]R. R. Sharma and S. Rodriguez, Phys. Rev. **153**, 823 (1967).
[48]H. Atzmüller, F. Froshl, and U. Schoeder, Phys. Rev. B **19**, 3118 (1979).
[49]H. J. Queisser and U. Heim, Annual Review of Materials Science **4**, 125 (1974).
[50]L. Mehrkam and F. Williams, Phys. Rev. B **6**, 3753 (1972).

Downloaded 02 Feb 2011 to 155.198.39.40. Redistribution subject to AIP license or copyright; see http://jap.aip.org/about/rights_and_permissions